machines

MDPI

Article

Displacement Analysis of Large-Scale Robotic Arm for Printing Cement Mortar Using Photogrammetry

Josef Brousek [1,*], Tomas Petr [1] and Radomir Mendricky [2]

[1] Department of Vehicles, Institute for Nanomaterials, Advanced Technology and Innovation, Technical University of Liberec, 461 17 Liberec, Czech Republic

[2] Department of Manufacturing Systems and Automation, Faculty of Mechanical Engineering, Technical University of Liberec, 461 17 Liberec, Czech Republic

* Correspondence: josef.brousek@tul.cz

Abstract: The development of specialised equipment for three-dimensional printing of cement mortar requires the deployment of advanced design methods. The accuracy of printing robotic arms is influenced by the change in the position of the end effector, which is influenced by the stiffness of the arm, or deformation of parts of the arm and yielding in the place of rotation axes. Determining the actual change in the end effector position is often a difficult challenge. In this paper, we analysed the displacement on a large robotic arm by the non-contact optical photogrammetry method. We applied this method to a specialised 2.8 m long robotic arm SCARA with an added rotational axis. We compared the results from photogrammetry with the results from measurements with a mechanical deflection meter, and with the predicted displacement values from the FEM simulation. The results from both measurement methods showed maximum deviations of hundredths of a mm. The findings of the analysis thus indicate that photogrammetry meets the strict requirements for displacement measurement on a robotic arm for the 3D printing of cement mortar. A significant advantage of the method is the possibility of measuring almost all attainable arm positions and achieving results in hundreds of places.

Keywords: robotic arm; printing cement mixtures; concrete printing; 3D printing; additive manufacturing; displacement analysis; photogrammetry

check for updates

Citation: Brousek, J.; Petr, T.; Mendricky, R. Displacement Analysis of Large-Scale Robotic Arm for Printing Cement Mortar Using Photogrammetry. *Machines* **2023**, *11*, 37. https://doi.org/10.3390/machines11010037

Academic Editor: César M. A. Vasques

Received: 8 November 2022
Revised: 22 December 2022
Accepted: 24 December 2022
Published: 29 December 2022

1. Introduction

Nowadays, three-dimensional printing techniques are becoming increasingly popular for construction applications [1]. Research and development in the field of printing cement mortar for construction purposes is currently dealt with by teams from different parts of the world, e.g., in the following projects: Apis Cor from the USA [2], Baumit BauMinator from Germany [3], Betabram from Slovenia [4] and FBR Ltd from Australia [5]. Major international companies operating in the conventional construction sector have also begun to invest in their own development in this area, e.g., Sika, Lafarge, Strabag, Skanska, etc. [6]. In most cases, the printing is performed by specialised robotic equipment developed to print layers of cement mortar. The layers are printed sequentially, one on top of the other, in such a way that the rate of solidification of the mixture is sufficient, and the printed layers can bear the weight of the newly added layers [7–9]. Robotic devices are currently being used for printing through various approaches. These approaches can fundamentally be divided into two groups. The first group uses universal industrial robotic solutions equipped with newly developed printheads for extruding the print mixture. This approach is used by the Baumit BauMinator project [3]; the advantage of this approach is the immediate availability of a robotic device capable of performing the required movement of the printhead. Limitations of an industrial robotic solution may lie in the insufficient spatial range that is necessary to realistically print buildings for conventional use in current and future society. The second development group focuses both on the development of the printhead and on the design of the robotic device itself. These devices are purposefully developed for the construction of buildings [10,11]. Robotic devices for printing cement mortars are either developed in the form of Cartesian robots, in the form of specialised robotic arms of various configurations, or completely different concepts such as a solution using a cable-driven parallel robot [12]. The development of various specialised devices often requires the deployment of advanced methods of design.

Three dimensional cement mortar printing provides opportunities to execute complex designs without additional costs [13]. In the research and development of printing cement mortars, great emphasis is placed on the accuracy of laying individual layers on top of each other for their adequate layer binding [6]. A change in the nozzle's linear movement can increase the mixture yield and lead to track stretching [14]. Poor printing can also result in a lower concrete density [15]. In terms of the printing equipment, the accuracy of laying the layers is mostly affected by a change in the position of the end effector during the printing itself. In printing with a robotic arm, this change in position is influenced by the stiffness of the arm, or by deformation of parts of the arm and yielding in the place of rotation axes. Therefore, this fact is an essential parameter in the robotic arm design when it is necessary to work with a compromise between the stiffness of the device's parts and their weight. This parameter is usually analysed during the design with the use of strength calculations. Our team, which deals with the research and development of complete printing of cement mortars for the construction of buildings at the Technical University of Liberec, is developing a printing solution with a specialised SCARA robotic arm with an added rotation axis. The length of the end effector on the final arm for the actual printing of buildings will be 5.6 m from the basic axis of rotation. We are currently validating this approach on a developed experimental 2.8 m long robotic arm, with the length of the individual arms in a 1:2 ratio to the size of the arms on the final arm. In the design of the experimental robotic arm, we assumed an acceptable displacement at the end of this arm of around 3 mm. We verified this assumption with an FEM simulation, which took into account the deformation of the individual parts of the arm, along with yielding in the axes of the motors. The results of predicted displacements from the design of the experimental arm are shown in Figure 1.

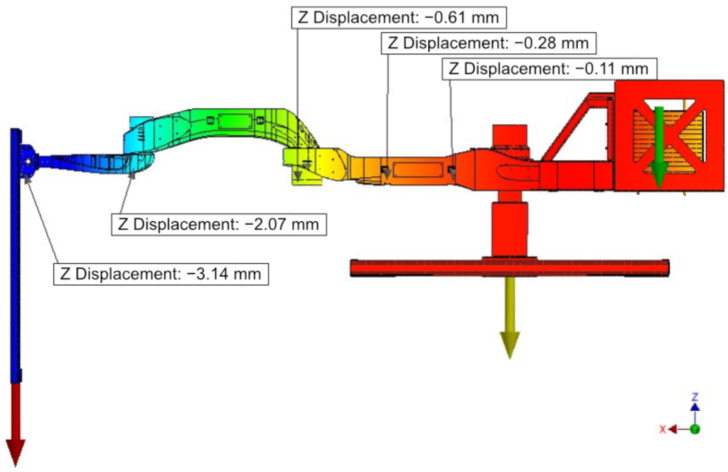

Figure 1. Results of predicted displacements from the design of the experimental arm, taking into account the deformation of individual parts of the arm and yielding in the axes of motors.

The actual amount of change in the position of the end effector on the arm is also influenced by the precision of the manufacturing and assembly of the robotic arm. The results of the simulations are also affected by the simplifications with which the computational analyses are performed. For the purpose of developing the printing device, we addressed the question of how great the change in the position of the end effector on the experimental robotic arm designed by us is. Another question was how it would be possible to measure and analyse the parameter in different positions with sufficient accuracy. Due to its design, dimensions and application for printing cement mortars, the arm is able to reach a relatively wide range of positions in space. The changes in positions in space are therefore quite significant, and it was necessary to choose a method that would be able to provide both comparable results as well as a comprehensive and effective inspection of displacement in a three-dimensional space. Measurement options for robotic arms include a single-purpose test platform equipped with a digital dial indicator and a tension/compression dynamometer, as was used in [16]. Another potential measurement solution is the deployment of inductive displacement sensors and therefore direct measurement on parts of the robotic arm [17]. However, these conventional measurement methods have rather extensive limitations for measurements on a robotic arm. It is very difficult to analyse multiple arm positions in a large workspace with them, and they can also only provide results at certain points precisely defined at the beginning of the measurement. Our team was looking for a solution that would enable a comprehensive analysis of the robotic arm.

Based on our experience with measurements in space, we proposed the use of the photogrammetry method to measure arm deformations, which, with the right approach, has the potential to provide the necessary results. The key idea of this paper is therefore the use of the photogrammetry method in addressing measurements on a large robotic arm. We see the potential of this method in the possibility of measuring in an almost unlimited number of arm positions, therefore providing all the necessary results for research and development of a robotic arm for printing cement mortars.

2. Methods

Photogrammetry enables measuring arm displacement in different arm positions, resulting in the necessary consistency and comparability of results. In order to verify the provided photogrammetry results from measuring on a large robotic arm, we performed a control measurement with a mechanical deflection meter. The control measurement was conducted in the initial position of the arm, in which the symmetric surfaces of all arms are in one plane. This position "I" is shown in Figure 2a.

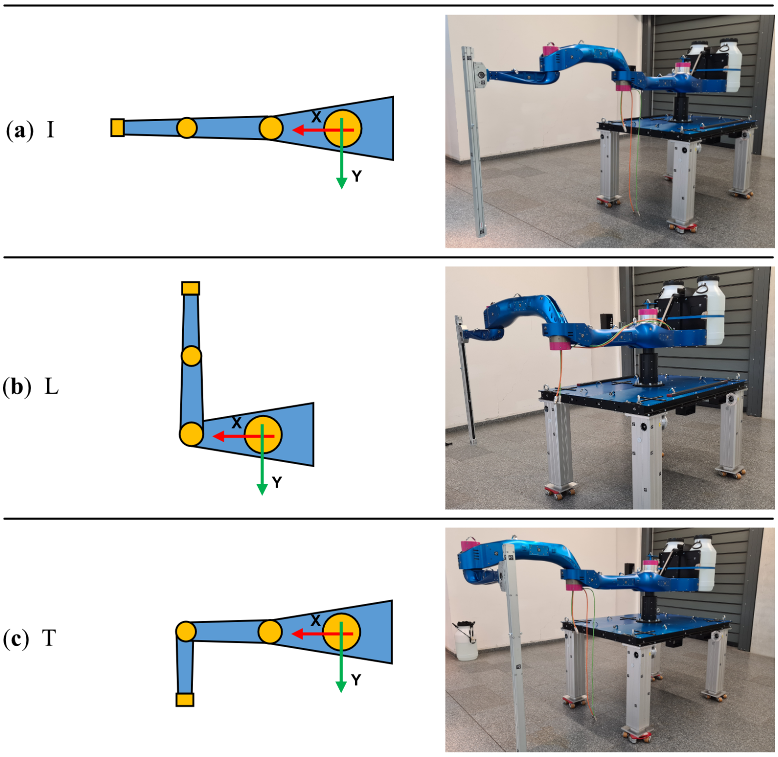

Figure 2. Robotic arm measuring positions: (**a**) Position "I", (**b**) Position "L", (**c**) Position "T".

The time sequence of individual measurements was as follows: In position "I", we first made measurements with the mechanical deflection meter. In this position, we then immediately measured with the photogrammetry and compared the results. Then we moved the robotic arm sequentially to positions "L" in Figure 2b and "T" in Figure 2c, which we measured with the photogrammetry.

The arm was designed for a maximum operating load of 35 kg on the end actuator. This load represents the maximum calculated weight of the printhead together with the cement mortar. We therefore performed the measurement in two states—unloaded (marked as State_1) and loaded (marked as State_2). In the unloaded state, the arm was left without a load on the end actuator, and in the loaded state, a 35 kg load was placed on the end actuator.

2.1. Description of Measured Points

We determined the measurement points on the robotic arm where it was possible to make comparable measurements by both methods, and these points were also distributed along the entire length of the arm. These were specifically five points illustrated in Figure 3. The points are defined by the longitudinal distance from the axis of rotation of the arm.

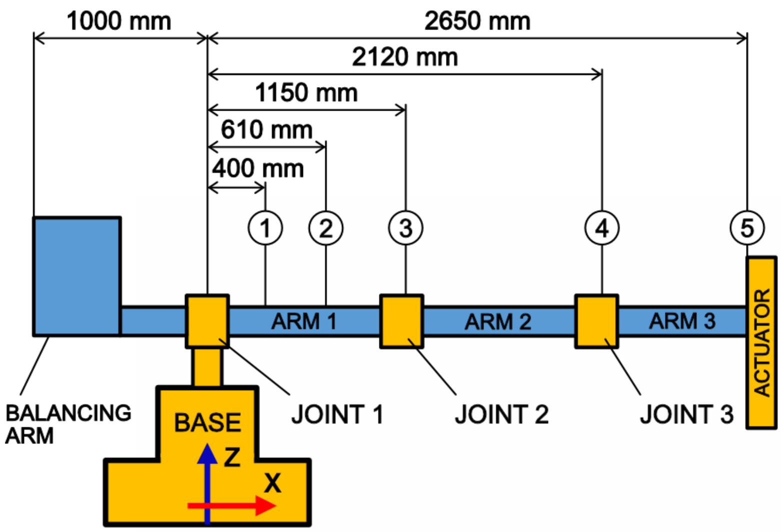

Figure 3. Diagram of the robotic arm with marked measurement points.

This is an experimental SCARA robotic arm with an added rotation axis. The robotic arm consists of three arms, a balancing arm, an end actuator and a base. Each part of the arm was designed through generative design, and they are made of an aluminium alloy with CNC chip machining technology. The parts of the arm are connected by means of Harmonic Drive rotary servo actuators with a harmonic gearbox. The structure of the balancing arm is made of steel welded parts combined with aluminium alloy elements. The weight on the balancing arm is made up of switchboards with the robot's control system. The working end of the arm contains an end actuator that enables a vertical lift up to a height of 1 m. The base of the robotic arm consists of welded steel elements and four lifting columns that enable a lift up to a height of 2.5 m.

Measurements on the robotic arm were carried out in the phase before the completion of the electronic control components, the position of which is designed as a counterweight to the end actuator. In Figure 3, this position is called the balancing arm. For measurement purposes, we placed two barrels with water in the position, the weight of which corresponded to the assumed weight of the switchboards, namely 98 kg, for which the arm was designed.

2.2. Description of Deflection Meter Measurements

We performed measurements with a mechanical deflection meter in a room at 21 °C at the specified measurement points; the deflection meter used was Kmitex CSN EN ISO 46325. The parameters of the deflection meter are listed in Table 1. First, we cleaned the measured point, then we placed the deflection meter stand in the corresponding position in the unloaded state of the arm. The stand was attached to the upper horizontal surface of the robotic arm base. The stem of the deflection meter always rested perpendicular to the horizontal surface on the robotic arm, so the results provided and listed are always relative to this horizontal surface of the base. We clamped the deflection meter in the stand and set the rotary dial to zero. Then, we loaded the end effector with a load of 35 kg and read the measured value of the vertical displacement from the meter. After this, we unloaded the arm and read the deflection meter again to verify that the arm was returning to its initial position. This is how we measured the values of vertical displacement at the five measurement points in position "I".

Table 1. Parameters of deflection meter Kmitex CSN EN ISO 46325.

Deflection meter	KMITEX CSN EN ISO 46325
Measuring range	0–10 mm
Measurement accuracy	0.01 mm

2.3. Description of Photogrammetry Measurement

For a comprehensive assessment of the spatial deformations of the robotic arm, an optical method was used—photogrammetry—which is based on the principle of passive triangulation. In photogrammetry, the object, or reference points located on it, is photographed from several positions and elevation levels (see Figure 4). In addition to regular 'uncoded' points, the images must also contain a sufficient number (at least five in each image) of unique 'coded' points and objects to determine the reference distance (e.g., reference bars). Photogrammetry can be used to inspect small objects (e.g., a few cm in size) as well as very large objects (on the order of several tens of meters). The limitations lie in the size of the reference points used (the recommendation is that the diameter of the point corresponds to at least 10 pixels on the CCD chip of the sensor), the use of reference bars of appropriate size and sufficient space around the object—for easy images taking. If the basic methodology is followed, the software is able to calculate the coordinates of the reference points in three-dimensional space with high accuracy (usually in hundredths of a mm [18]) based on the set of 2D photographs taken. If we take a series of images in individual positions of the arm in a loaded and unloaded state, then we can monitor the displacement (deformation) of the reference points when the arrangement of the arms is changed, or after the end effector of the robotic arm is loaded.

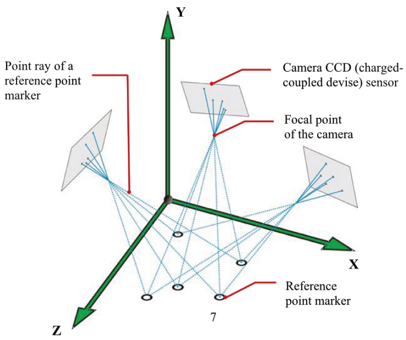

(**a**)

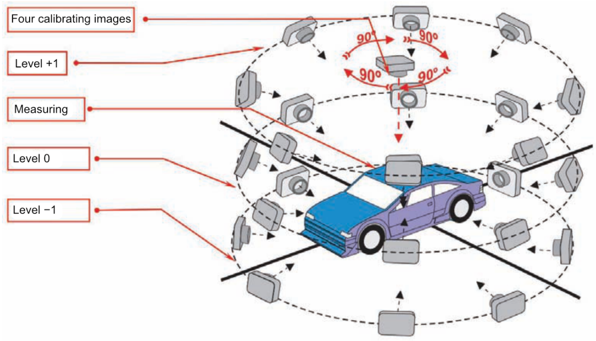

(**b**)

Figure 4. Principle of the photogrammetry method: (**a**) Beams of reference points in three images [19]. (**b**) Method of photographing large objects [20].

The TRITOP (GOM GmBH, Braunschweig, Germany) photogrammetry system was used for the measurement. This is a non-contact optical measuring system that is used in the field of quality control and deformation analysis. Description of the TRITOP system:

- Camera: Nikon D500 (Nikon Imaging Japan Inc., Tokyo, Japan), resolution: 21 Mpx;
- Lens: Titanar 24 mm, f = 2.8;
- Calibration bars: 1 m, carbon (2 pcs);
- Coded and uncoded reference points ∅ 5 mm;
- According to the acceptance test performed pursuant to VDI 2634 Part 1 [21], the maximum measurement deviation with the mentioned device for the 'Length measurement error' parameter is up to 0.033 mm and the average deviation for the Scale bar 0.25–1 m is 0.009 mm.

The measuring system was set before the actual measurement according to the manufacturer's recommendations [22] (aperture F11, shutter speed 1/250 s). Scene preparation for photogrammetry is shown in Figure 5. Taking into account the size of the robotic arm, the size of the calibration bars used, the diameter of the reference points, the range of the flash, the required resolution and the spatial layout, an approximate imaging distance of 3 m was chosen (the lens was manually focused at this distance). First, four calibration pictures were taken (from one position, turning the camera by 90°), and then about 20 pictures were taken from each of the five height levels, i.e., a total of at least 100 images for each measurement series (Figure 6). The complete measurement statistics are provided in Table 2.

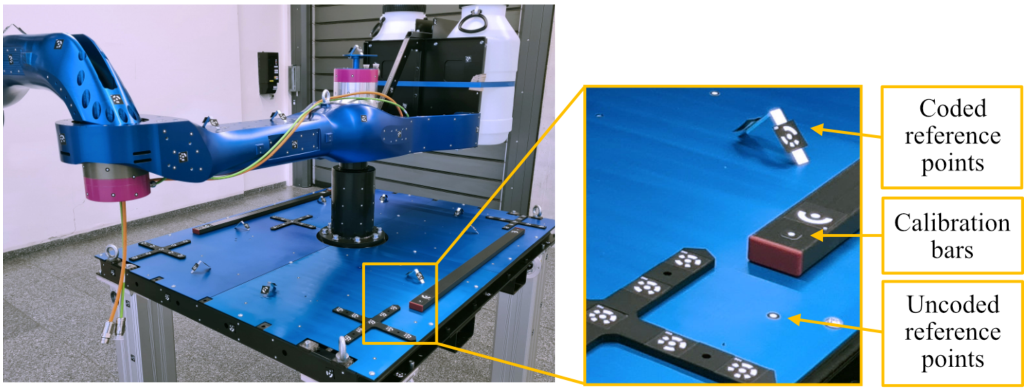

Figure 5. Preparing a scene for photogrammetry.

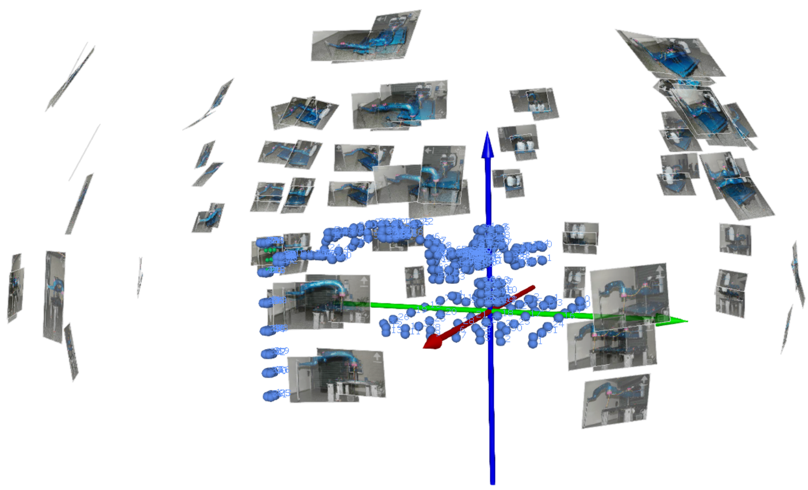

Figure 6. Camera positions when taking pictures/calculated point components of the robotic arm.

Table 2. Photogrammetry statistics.

Arm Position	Total Number of Images (pcs)	Average Theoretical Point Precision (mm)	Average Image Point Deviation (Pixel)	Average Reference Point Deviation (mm)	Number of Coded Reference Points [pcs]	Number of Uncoded Reference Points (pcs)	Average Scale Bar Discrepancy (mm)
I_1	177	0.009	0.062	0.029	180	451	0.007
I_2	138	0.009	0.062	0.029	176	438	0
L_1	102	0.012	0.062	0.029	180	432	0.015
L_2	107	0.009	0.063	0.029	179	425	0.001
T_1	109	0.011	0.063	0.03	178	437	0.01
T_2	112	0.01	0.061	0.029	179	439	0.011

GOM ATOS Professional 2018 SW (GOM GmBH, Braunschweig, Germany) was used for image processing, the definition of point components and a subsequent inspection. After the images were oriented, the positions of the uncoded points in 3D space were calculated in the software. These points were used to determine 'point components', which represent individual important parts of the robotic arm (arms, rotation axes, table, actuator, etc.). After this, they were aligned to a uniform coordinate system, the origin of which was defined at the intersection of the table plane and the axis of the main arm (Axis_1). The positive direction of the z-axis was perpendicular to the table in an upward direction, and the x-axis in the direction of Arm 1. All six series were processed in this way as Stages in one project. This enabled changing the reference Stage and searching for relative deformations between individual states. Displacements of points in the same places where deflection meter measurements were conducted were primarily calculated. The measurement was conducted both for arm position "I" and the remaining two positions "L" and "T". After inspection and verification with conventional measurements, a total analysis of the displacements of individual components in the z-axis (caused by the deformation of the arms and the yielding of axial connections after the load was placed on the actuator) was performed. Angle changes in the longitudinal and transverse directions of each arm were also measured. This helped to better verify and understand which axes contribute the most to the overall displacement of the end effector of the robotic arm.

3. Results

3.1. Deflection Meter Results

The results of displacements in the z-axis from individual points of the robotic arm measured by a mechanical deflection meter are shown in Table 3. The vertical displacement at the first measurement point, which was located at the shortest measured distance of 400 mm from the central axis of the arm, was −0.16 mm. Conversely, at the farthest measurement point from the central axis, i.e., at a distance of 2650 mm, the vertical displacement was −3.14 mm. The measurement checked whether there was any permanent deformation of the arm. Table 3 therefore also includes values from the deflection meter before loading and after unloading the robotic arm. The vertical displacement values themselves are also shown in the graph in Figure 7.

Table 3. Results of displacement measurements in the *z*-axis with a mechanical deflection meter.

Marked Measuring Point	Distnce of the Measuring Point from the Axis (mm)	Value on the Deflection Meter before Loading (mm)	Value on the Deflection Meter after Loading (mm)	Value on the Deflection Meter after Unloading (mm)
1	400	0	−0.16	0
2	610	0	−0.29	0
3	1150	0	−0.66	0
4	2120	0	−2.02	0
5	2650	0	−3.14	0

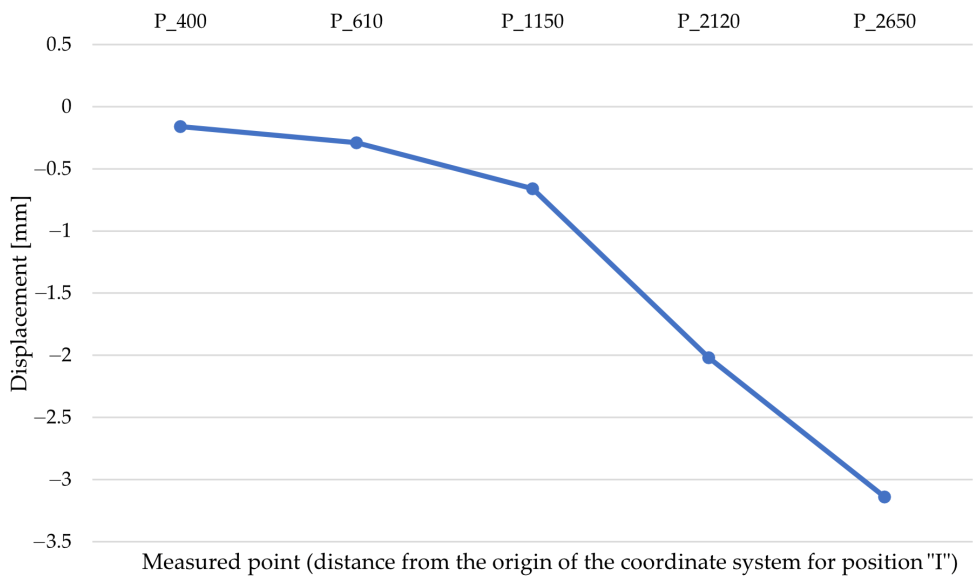

Figure 7. Results of displacement measurements in the *z*-axis with a mechanical deflection meter.

3.2. Photogrammetry Results

3.2.1. Results in Points Comparable to the Results from the Deflection Meter

In the first step, the displacements of the robotic arm in the *z*-axis were evaluated in the same places where the deflection meter measurement was performed. To ensure greater reliability, two reference points were evaluated for each such location, placed symmetrically from the XZ plane. The displacement vectors of the selected points for the position “I” are shown in Figure 8 and Table 4. It is evident that the displacement vectors of each pair of points coincide with the “I” position in each of the examined locations, with a maximum difference of 0.02 mm. Arithmetic means of the two values were also taken as reference values for verification with manual measurement for each evaluated location. For completeness, Table 4 and Figure 9 below show a summary of measurement results for the other two states as well.

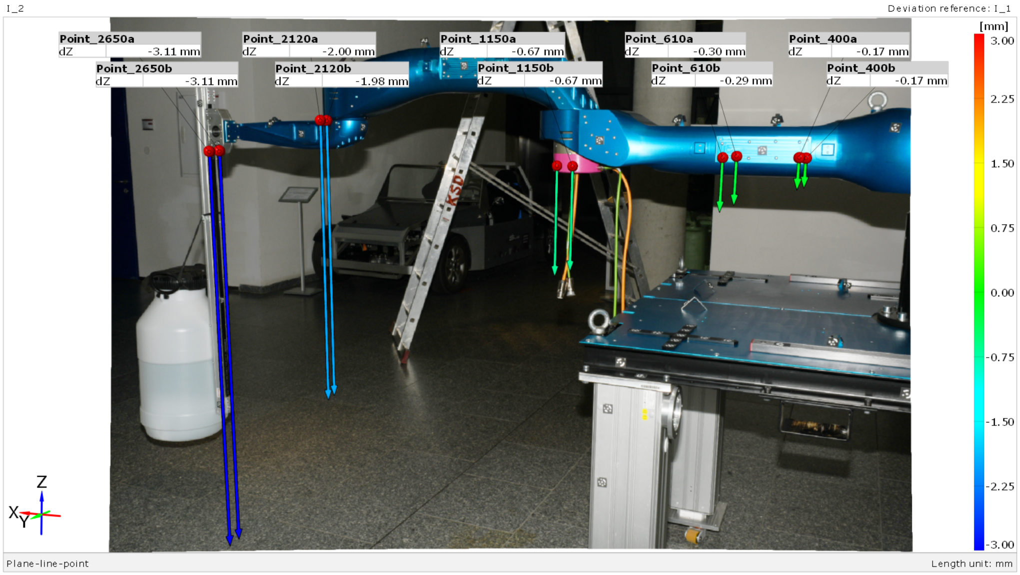

Figure 8. Displacements (deformations) of selected points in places measured by a deflection meter (State I_2 vs. I_1).

Table 4. Results of *z*-axis displacement photogrammetry measurements.

Arm Position/Measured Point/Displacement (mm)	P_400	P_610	P_1150	P_2120	P_2650
I_2 (a)	−0.17	−0.3	−0.67	−2	−3.11
I_2 (b)	−0.17	−0.29	−0.67	−1.98	−3.11
L_2 (a)	0.01	−0.02	−0.08	−1.33	−2.38
L_2 (b)	−0.06	−0.1	−0.17	−1.32	−2.39
T_2 (a)	−0.18	−0.26	−0.5	−1.26	−2.09
T_2 (b)	−0.13	−0.21	−0.46	−1.29	−2.15

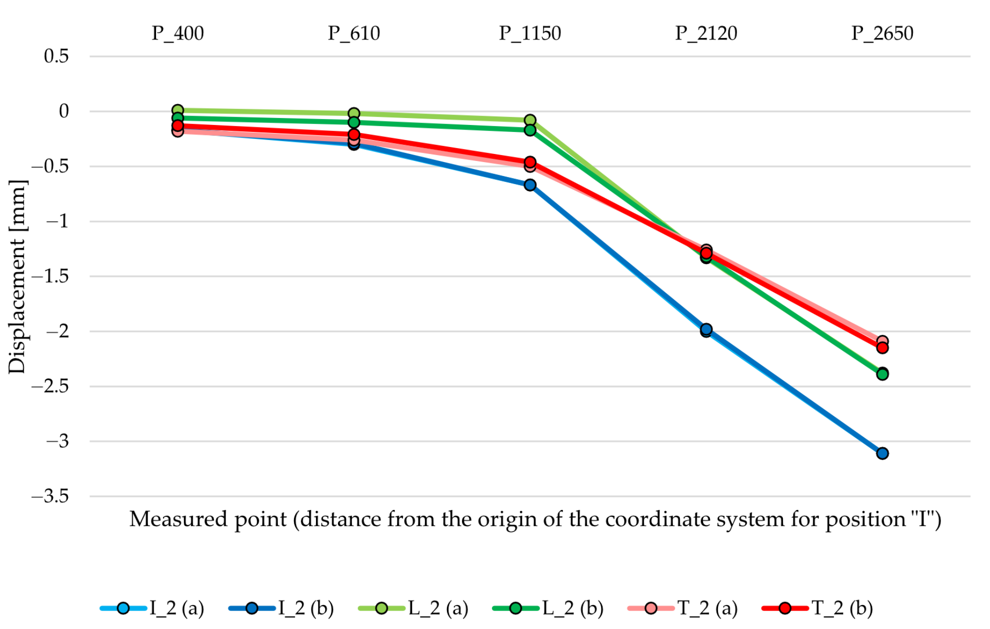

Figure 9. Results of *z*-axis displacement photogrammetry measurements.

3.2.2. Comparison of Values Measured with a Deflection Meter and Photogrammetry

Table 5 shows a comparison of the values obtained with a deflection meter and photogrammetry. The smallest difference in results between both measurement methods was achieved in the first three measurement points (1, 2, 3), with a difference of 0.01 mm. On the contrary, the biggest difference was found in the last two measured points (4 and 5), with a difference of −0.03 mm.

Table 5. Comparison of results measured with a deflection meter and photogrammetry.

Marked Measuring Point	Distance of the Measuring Point from the Axis (mm)	Vertical Displacement (Deflection Meter) (mm)	Vertical Displacement (Photogrammetry) (mm)	Difference between Deflection Meter and Photogrammetry (mm)
1	400	−0.16	−0.17	0.01
2	610	−0.29	−0.3	0.01
3	1150	−0.66	−0.67	0.01
4	2120	−2.02	−1.99	−0.03
5	2650	−3.14	−3.11	−0.03

For clarity, the resulting differences between deflection meter and photogrammetry measurements are shown in the following Figure 10.

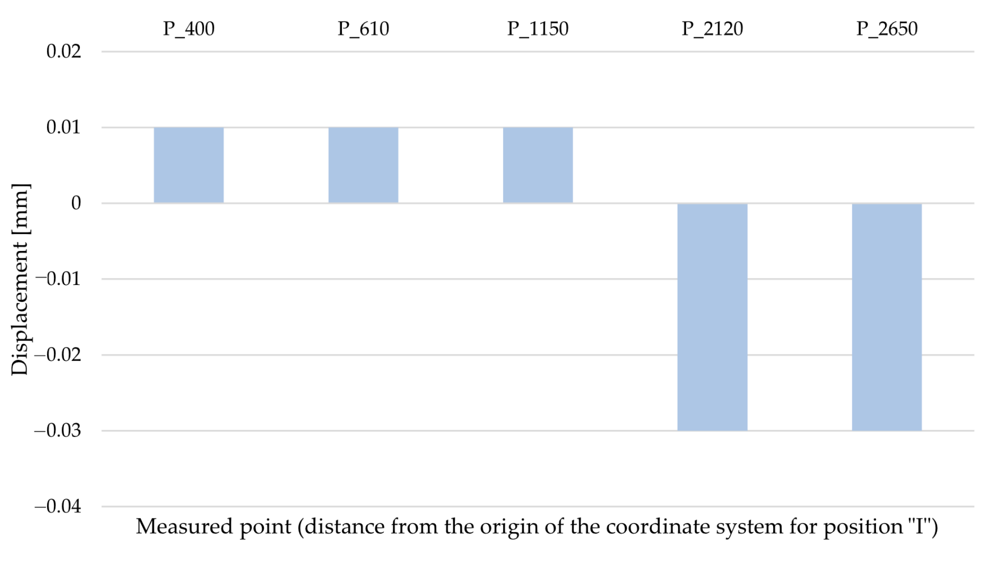

Figure 10. Differences between deflection meter and photogrammetry measurements.

3.2.3. Overall Results Provided by Photogrammetry in Three Arm Positions

Figure 11 shows a comprehensive analysis of the displacement of individual arms when the end actuator is loaded with 35 kg in the "I" position. Positions "L" and "T" were evaluated in the same way. The maximum displacement values of all four monitored components (arm 1–3 and actuator) for all three monitored arm configurations are shown in Figure 12.

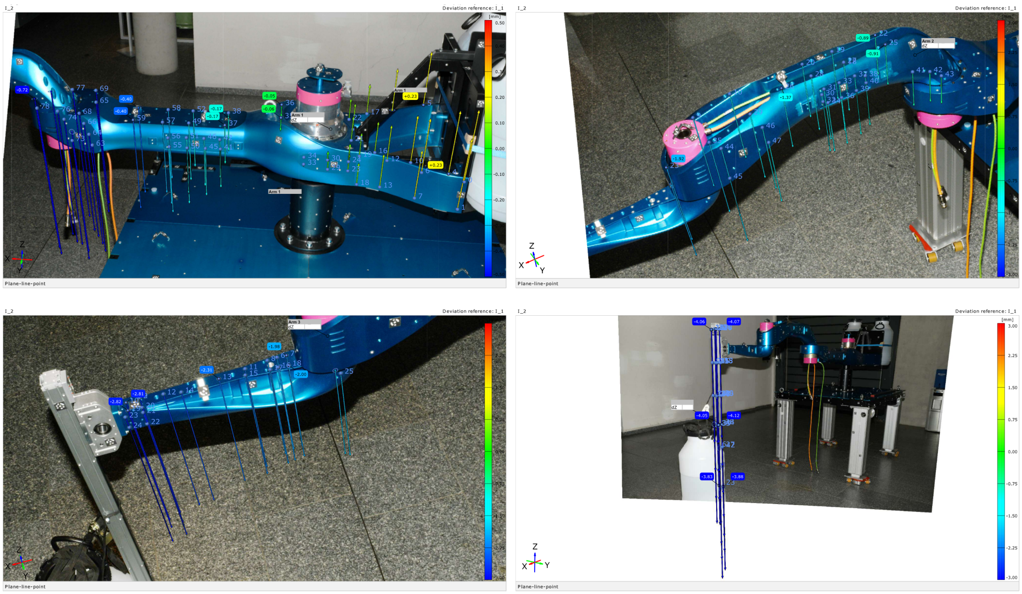

Figure 11. XY displacements of point components of Arms 1–3 and the actuator in the z-axis (State I_2 vs. I_1).

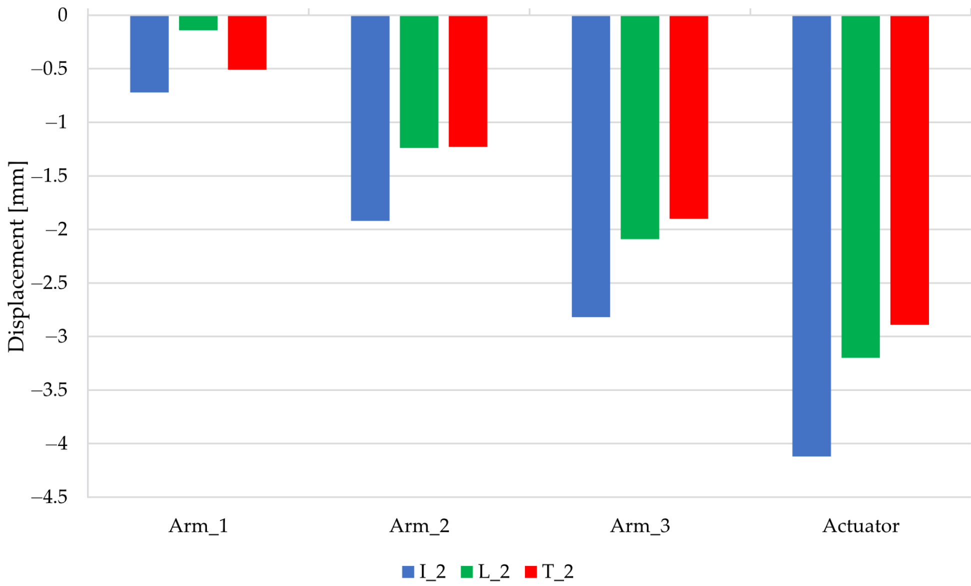

Figure 12. Maximum displacement of the component in the z-axis (State_2 vs. State_1).

3.2.4. Inspection of Angle Measurement

In addition to absolute displacements, angles were also measured in two directions—longitudinally with the arm and perpendicular to this direction (transversely). The longitudinal angle shows the tilting of the arm in the direction of its axis, and the transverse angle shows the 'twisting' with a torsion load. This occurs if the load is deflected off the x-axis, i.e., if any of the following arms is rotated by a non-zero angle to the x-axis; in our case, the maximum possible angle is 90°. In position "L", Arm_1 (or Axis_1) is loaded in this way, and in position "T", Arm_1 and Arm_2 (or Axis_1 and Axis_2) are loaded in the transverse direction. The inspection of angle measurements is shown in Figure 13.

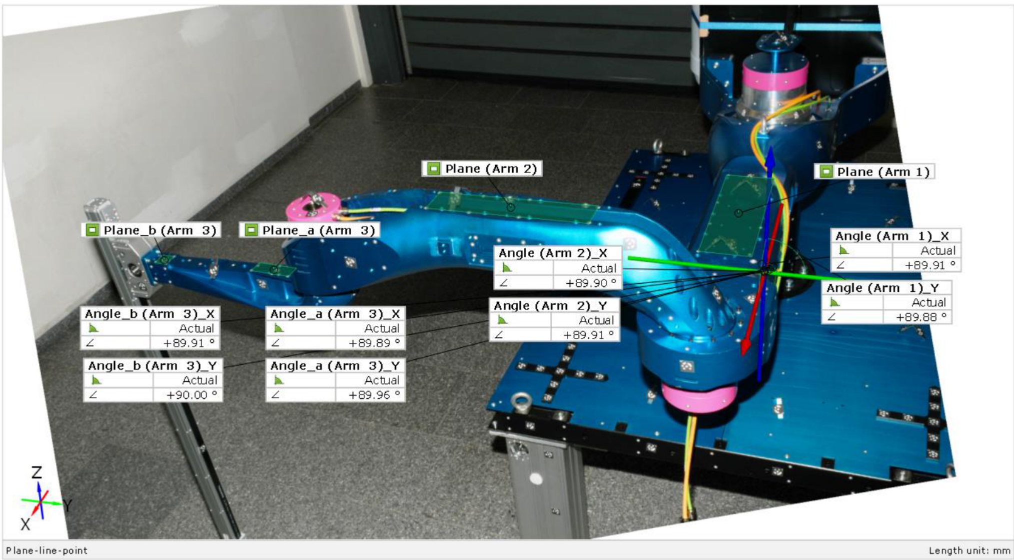

Figure 13. Arm angle measurement (measured between the normal to the plane and the corresponding axis of the coordinate system) (Position "L_1").

The following Table 6 shows the comprehensive results of this analysis. It shows the deviations of individual arms from the horizontal plane, both in the direction of the arm (axial direction) and perpendicular to this direction (cross direction). For clarity, it also shows which axis of the absolute coordinates for the given arm configuration this direction corresponds to (X or Y). A negative value of the angle in the longitudinal direction means a downward deviation from the horizontal plane, and a negative angle for the transverse direction represents a clockwise rotation (when viewed from the front on the given axis).

Table 6. Total angular deviations of each arm from the horizontal plane.

Arm Position	Angle of Arm 1 Axial (deg)		Angle of Arm 1 Cross (deg)		Angle of Arm 2 Axial (deg)		Angle of Arm 2 Cross (deg)		Angle of Arm 3 Axial (deg)		Angle of Arm 3 Cross (deg)	
I_1	X	−0.09	Y	−0.13	X	−0.13	Y	−0.13	X	−0.19	Y	−0.13
I_2	X	−0.13	Y	−0.13	X	−0.21	Y	−0.14	X	−0.31	Y	−0.15
L_1	X	−0.09	Y	−0.12	−Y	0.09	X	−0.1	−Y	0.02	X	−0.1
L_2	X	−0.09	Y	−0.1	−Y	0.02	X	−0.11	−Y	−0.09	X	−0.12
T_1	X	−0.09	Y	−0.13	X	−0.13	Y	−0.14	Y	−0.18	−X	0.17
T_2	X	−0.12	Y	−0.15	X	−0.17	Y	−0.18	Y	−0.27	−X	0.21

The results in Table 6 show the absolute rotation angles of each arm. The error affects both production and assembly inaccuracies, as well as any deformations caused by the weight of individual components. In order to precisely determine the effect of loading of the actuator with 35 kg, the difference between the loaded (State_2) and unloaded states (State_1) was calculated and these values were entered in Figure 14.

For example, it is evident in the "I" arm position (blue bars) that as the number of joints and the total length of the arm chain increases, so does the longitudinal rotation (tilt). In arm 1, it is −0.04 mm, whereas in arm 3, it is −0.12 mm. This angle naturally includes the deformation of the third, second and first joints and any deformations of these arms. The average rotation from each segment in this case is −0.04 mm (also verified by an analysis of the relative deformations and tilts of the arms), and it also shows that the stiffness of the joints (motors) and individual arms is uniform with regard to the stress in the given place. It should be noted that an angle change of 0.05° over a length of 2.5 m is a displacement of 2.2 mm. The angular changes therefore only confirm the displacements found in the previous analysis.

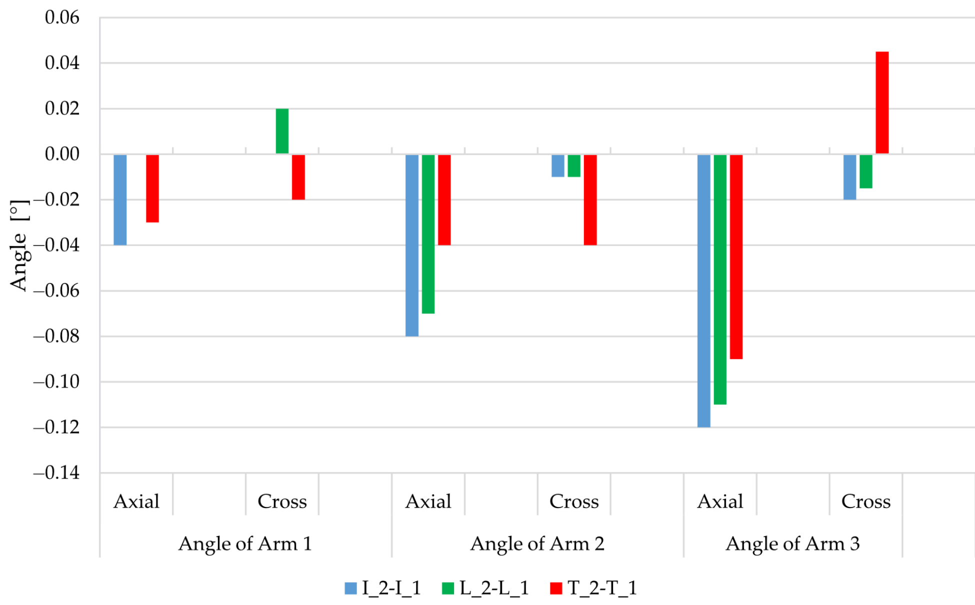

Figure 14. Change in arm angle after actuator loading (State_2–State_1).

4. Discussion

In this article, we analysed the application of an adequate method for measuring end actuator displacement in the vertical *z*-axis on an experimental robotic arm designed by us for the development and research of the 3D printing of cement mortars. At the beginning of the article, we asked ourselves what method would provide comprehensive and sufficiently accurate displacement results in the extensive three-dimensional workspace of the robotic arm.

We measured the displacement at five points on the arm in the basic "I" position, i.e., in the position in which all three parts of the arm are in zero rotation, with a mechanical deflection meter and the use of the photogrammetry method. A comparison of the results obtained from both methods has shown very good concordance. Deviations do not exceed hundredths of a mm and are almost negligible in terms of the absolute displacement values on the arm. Based on these results and the measurement itself, we believe that the non-contact optical photogrammetry method meets the strict requirements for the displacement measurement on a robotic arm designed for the 3D printing of cement mortars; it is possible to achieve virtually the same results as those provided by a mechanical deflection meter. However, compared to photogrammetry, measurements with a mechanical deflection meter have significantly limited possibilities of measuring in challenging positions, which the SCARA robotic arm with an added rotation axis is capable of doing. Conversely, photogrammetry has a significant advantage in measuring almost all the arm positions of the device in the 3D printing of cement mortars. It is also not necessary to place any additional dimensional elements on the arm that would limit its movement, as is the case with a mechanical deflection meter. Based on the concordance of the results from the mechanical deflection meter and photogrammetry measurements in the "I" position, we believe that the results from photogrammetry measurements in the "L" and "T" positions can be considered adequate with a high probability.

Another essential question was how large the displacement of the end actuator on the arm is compared to the assumptions and simulation results from the arm design. As the last column of Table 7 shows, the absolute values of the differences between vertical displacements from the simulation and the results from photogrammetry in the "I" position were in a range of hundredths of millimetres. The maximum difference was an absolute value of 0.08 mm. This finding suggests that with an adequate approach, the displacement simulation on this type of robotic arm can achieve results that are relatively consistent with real values. This concordance also indicates that the expected tolerances were fairly precisely observed in the manufacture and assembly of the robotic arm.

Table 7. Comparison of photogrammetry and simulation results.

Marked Measuring Point	Distance of the Measuring Point from the Axis (mm)	Vertical Displacement (Photogrammetry) (mm)	Vertical Displacement (Simulation) (mm)	Difference between Simulation and Photogrammetry (mm)
1	400	−0.17	−0.11	0.06
2	610	−0.3	−0.28	0.02
3	1150	−0.67	−0.61	0.06
4	2120	−1.99	2.07	−0.08
5	2650	−3.11	−3.14	−0.03

The reason for the displacements is mainly bending deformations of the arms and deformations of the axes bearings (resulting from their stiffness and the total load of the mass itself and the loads on the actuator). The absolute magnitude of the deviations is expected (predicted by the numerical calculations), and it is not always the aim to excessively increase the stiffness of the whole structure and the axes connections to minimize these errors. This would lead to a further increase in weight and moments of inertia, and the reduced dynamics would have to be compensated by higher motor power, consequently increasing the cost of the whole device. We aim to have a reliable method to measure these deviations and design a feedback control to actively compensate for this error with software, if necessary.

In addition to absolute displacements, which are mostly important in terms of 3D printing accuracy, in an analysis of the behaviour of the SCARA robot, it is also appropriate to observe how the arms twist due to the torsional flexibility of the joints after the actuator is loaded, or what their longitudinal and transverse inclination (angle) to the horizontal plane is. The results of the present study also suggest that this measurement enables us to determine the changes between loaded and unloaded states, as well as any inaccuracies in the assembly of the robot itself and the effect of the weight of each arm on the deformation of the joints. The information can thus be used to correct the assembly of the robotic arm.

5. Conclusions

The evidence from this study suggests that an analysis of deformations and displacements with the photogrammetry method on a large robotic arm for 3D printing of cement mortars offers significant benefits compared to traditional measurement tools. The results show that photogrammetry not only provides results in a few discrete points, but at hundreds of locations in three-dimensional space and a variety of robotic arm positions.

Further research could potentially explore the use of photogrammetry measurement results for the further development of the 3D printing of cement mortars with a robotic arm. The results could specifically be used as a basis for end effector position control corrections in the robotic arm control system. Further research could also assess the effect of lightening the printhead on the end effector of the arm. Photogrammetry measurements combined with verified end effector displacement simulation results can be recommended for the continued development, design and verification of the design of other robotic arms for the 3D printing of cement mortars. In a broader context, the photogrammetry method can be characterised as a beneficial tool in analysing displacement on a robotic arm that provides significant opportunities for the research and development of the 3D printing of cement mortars to improve the achieved quality of printed objects.

Author Contributions: Conceptualisation, J.B. and T.P.; methodology, J.B. and T.P. and R.M.; resources, J.B., T.P. and R.M.; validation, J.B., T.P. and R.M.; visualisation, T.P. and R.M.; writing—original draft preparation, J.B., T.P. and R.M. All authors have read and agreed to the published version of the manuscript.

Funding: The research presented in this paper was supported by the European Structural and Investment Funds of the Operational Programme Research, Development and Education within the project "3D Print in civil engineering and architecture—3D STAR" *reg. number CZ.02.1.01/0.0/0.0/16_025/0007424.

Data Availability Statement: All data presented in this study are included in the paper.

Acknowledgments: The research presented in this paper was supported by the European Structural and Investment Funds of the Operational Programme Research, Development and Education within the project "3D Print in civil engineering and architecture—3D STAR" reg. number CZ.02.1.01/0.0/0.0/16_025/0007424.

Conflicts of Interest: The authors declare no conflict of interest.

References

1. Shakor, P.; Nejadi, S.; Paul, G. A Study into the Effect of Different Nozzles Shapes and Fibre-Reinforcement in 3D Printed Mortar. *Materials* **2019**, *12*, 1708. [CrossRef] [PubMed]
2. Apis Cor. Apis Cor. Available online: https://www.apis-cor.com/ (accessed on 21 October 2022).
3. Baumit. Baumit BauMinator®. Available online: https://baumit.at/bauminator?PageSpeed=noscript (accessed on 21 September 2022).
4. BetAbram. Betabram.™ —Absolutely Simple, Fascinating and Magical to Use. Available online: https://betabram.com/ (accessed on 24 September 2022).
5. FBR Ltd. FBR | Industrial Automation Technology. Available online: https://www.fbr.com.au/ (accessed on 27 September 2022).
6. Partnerskabet 3D Printet Byggeri. 3D Printet Byggeri—Afslutningsrapport Februar 2018. Technical Report, 2018. Available online: http://3dprintetbyggeri.dk/pdf/Afslutningsrapport.pdf (accessed on 21 September 2022).
7. Craveiro, F.; Nazarian, S.; Bartolo, H.; Bartolo, P.J.; Pinto Duarte, J. An automated system for 3D printing functionally graded concrete-based materials. *Addit. Manuf.* **2020**, *33*, 101146. [CrossRef]
8. Khoshnevis, B. Toward Total Automation of On-Site Construction—An Integrated Approach Based on Contour Crafting. In Proceedings of the 20th ISARC, Eindhoven, The Netherlands, 21–24 September 2003. [CrossRef]
9. Panda, B.; Noor Mohamed, N.A.; Paul, S.C.; Bhagath Singh, G.; Tan, M.J.; Šavija, B. The Effect of Material Fresh Properties and Process Parameters on Buildability and Interlayer Adhesion of 3D Printed Concrete. *Materials* **2019**, *12*, 2149. [CrossRef] [PubMed]
10. Guamán-Rivera, R.; Martínez-Rocamora, A.; García-Alvarado, R.; Muñoz-Sanguinetti, C.; González-Böhme, L.F.; Auat-Cheein, F. Recent Developments and Challenges of 3D-Printed Construction: A Review of Research Fronts. *Buildings* **2022**, *12*, 229. [CrossRef]
11. Rehman, A.U.; Kim, J.H. 3D Concrete Printing: A Systematic Review of Rheology, Mix Designs, Mechanical, Microstructural, and Durability Characteristics. *Materials* **2021**, *14*, 3800. [CrossRef] [PubMed]
12. Tho, T.P.; Thinh, N.T. Using a Cable-Driven Parallel Robot with Applications in 3D Concrete Printing. *Appl. Sci.* **2021**, *11*, 563. [CrossRef]
13. Khajavi, S.H.; Tetik, M.; Mohite, A.; Peltokorpi, A.; Li, M.; Weng, Y.; Holmström, J. Additive Manufacturing in the Construction Industry: The Comparative Competitiveness of 3D Concrete Printing. *Appl. Sci.* **2021**, *11*, 3865. [CrossRef]
14. Elistratkin, M.; Alfimova, N.; Podgornyi, D.; Olisov, A.; Promakhov, V.; Kozhukhova, N. Influence of Equipment Operation Parameters on the Characteristics of a Track Produced with Construction 3D Printing. *Buildings* **2022**, *12*, 593. [CrossRef]
15. Le, T.; Austin, S.; Lim, S.; Buswell, R.; Law, R.; Gibb, A.; Thorpe, T. Hardened properties of high-performance printing concrete. *Cem. Concr. Res.* **2012**, *42*, 558–566. [CrossRef]
16. Wei, W.; Cai, G.; Gong, J.; Peng, S. Modeling and Analysis of the Stiffness Distribution of Host–Parasite Robots. *IEEE Access* **2021**, *9*, 86300–86320. [CrossRef]
17. Ștefan, A.; Grigore, L.; Oncioiu, I.; Constantin, D.; Mustață, Ș.; Toma, V.F.; Molder, C.; Gorgoteanu, D. Influence of the Stiffness of the Robotic Arm on the Position of the Effector of an EOD Robot. *Electronics* **2022**, *11*, 2355. [CrossRef]
18. Klus, P. The Theoretical and Actual Measurement Accuracy of TRITOP Photogrammetry System. Diploma Thesis, Brno University of Technology, Brno, Czech Republic, 2018.
19. Goda, I.; L'Hostis, G.; Guerlain, P. In-situ non-contact 3D optical deformation measurement of large capacity composite tank based on close-range photogrammetry. *Opt. Lasers Eng.* **2019**, *119*, 37–55. [CrossRef]
20. Gmurczyk, G.; Reymer, P.; Kurdelski, M. Global Fem Model of Combat Helicopter. *J. Kones Powertrain Transp.* **2011**, *18*, 9.

21. GOM GmbH. *GOM Acceptance Test (Certificate): Acceptance/Reverification According to VDI/VDE 2634*; GOM GmBH: Braunschweig, Germany, 2012.
22. GOM GmbH. *TRITOP*; Product Information, Nikon D500; GOM GmBH: Braunschweig, Germany, 2018.